Supplementary Information

Grain Boundary Optimization in Li–Mg Alloy Anodes via Controlled Cooling Rates and Cold Rolling

Chae Yeon Yeom, Woo Seok Choi, Seung Ho Lee, Jong Hoon Kimand Jong Hyeon Lee*

	Plane (hkl)	$\sin^2\theta$	$h^2 + k^2 + l^2$	a (Å)
Pure Li	**(110)**	**0.0955**	**2**	**3.5100**
	(200)	**0.1850**	**4**	
	(211)	**0.2846**	**6**	
Pristine Li–Mg alloy	**(110)**	**0.0959**	**2**	**3.5121**
	(200)	**0.1857**	**4**	
	(211)	**0.2854**	**6**	
Li–Mg alloy after Li stripping	**(110)**	**0.0986**	**2**	**3.5013**
	(200)	**0.1897**	**4**	
	(211)	**0.2927**	**6**	

Fig. S1. Lattice parameter changes with Li content.

Changes in the lattice parameter with varying Li content in the solid solution were observed. By converting the 2θ values to $\sin^2\theta$, the lattice constants for each diffraction plane were calculated using the least squares method. The results showed that the lattice constants for pure Li, the Li–Mg alloy, and the Li–Mg alloy after Li stripping were 3.5100, 3.5121, and 3.5033 Å, respectively. These values indicated that significant changes occur in the lattice constants during the alloying and delithiation processes. The lattice parameter of the pristine Li–Mg alloy was larger than that of pure Li owing to the incorporation of large Mg atoms into the Li lattice. Conversely, the lattice parameter after Li stripping was smaller than that of pure Li possibly because of is likely the formation of a compact solid solution of residual Li and Mg, whose hexagonal close packed structure is characterized by a small lattice constant (a,b = 3.2094 Å).

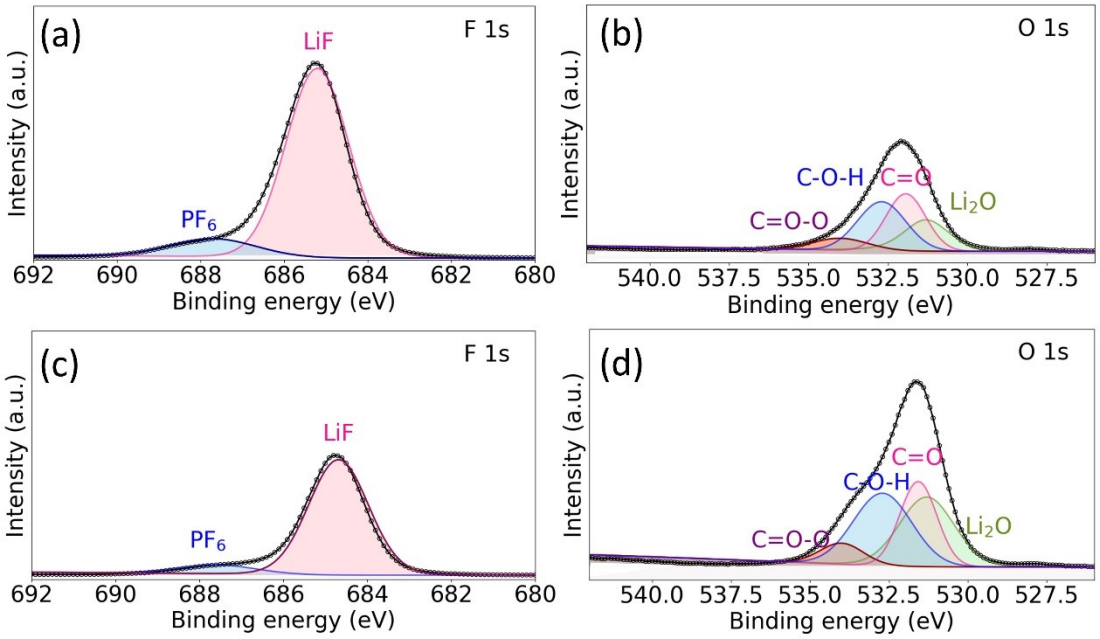

Fig. S2. XPS analysis of Li metal before cycling (immersing in electrolyte for one day): (a) F 1s spectrum, (b) O 1s spectrum; XPS analysis of Li metal after 10 cycles (c) F 1s spectrum, (d) O 1s spectrum.

Analysis of the XPS data before and after cycling of Li metal revealed that the intensity of LiF, as indicated by the F 1s peak, decreased after cycling as compared to that of the Li–Mg alloy. This suggests that the Li–Mg alloy may offer superior chemical stability compared to that of pure Li metal. Moreover, the increase in the intensity of Li_2O after cycling was relatively lower for Li metal than for the Li–Mg alloy, indicating more stable SEI formation and superior cycling characteristics in the Li–Mg alloy as compared to that of the Li metal.

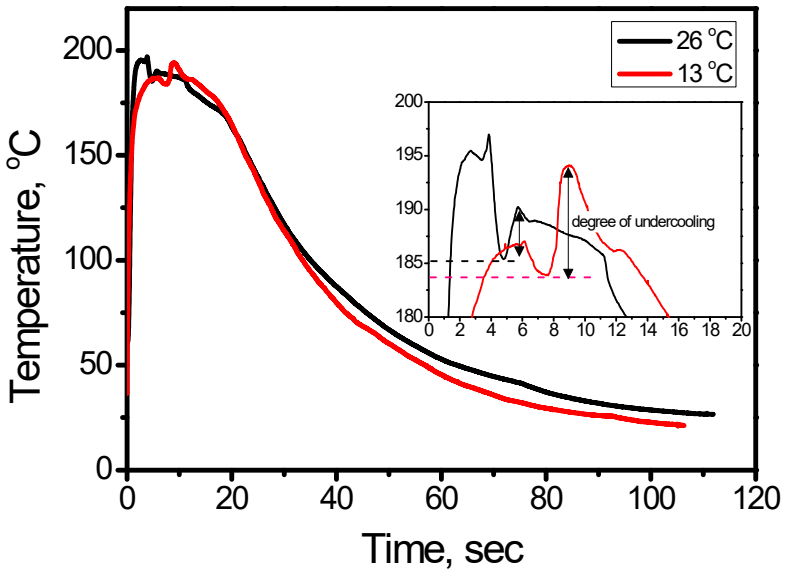

Fig. S3. Cooling curves depending on initial mold temperature.

The metal temperature was set to 200 °C, and the casting mold temperatures were set to: 26 and 13 °C for fast cooling. During cooling at 26 and 13 °C, the degrees of undercooling were 4.86 and 10.25, respectively, indicating that small grains formed at 13 °C.

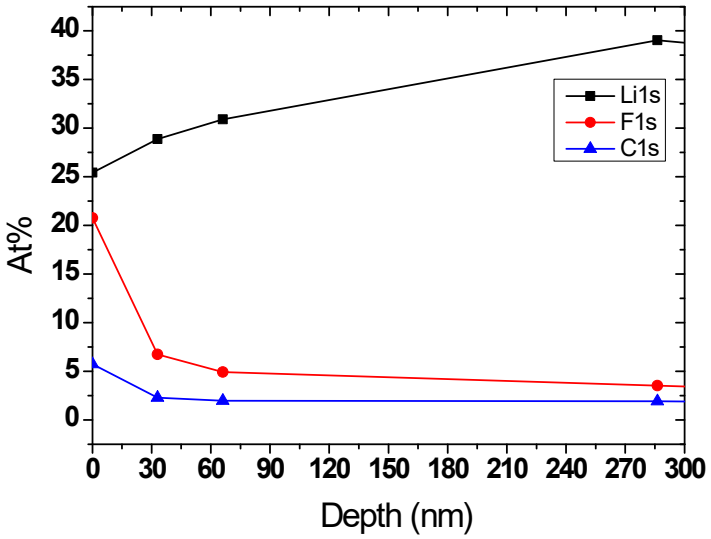

Fig. S4. Depth profiles derived from the XPS data of the SEI layer formed on the Li–Mg alloy anode.

The thickness of the SEI layer was approximately 66 nm, which was estimated from the XPS depth profiling data. The depth profile showed a decrease in the intensities of the SEI components (F and C) and a corresponding increase in Li intensity. These intensity changes corresponded to the boundary between the SEI layer and underlying material, allowing the determination of the SEI layer's thickness. The XPS depth profile was measured under the following conditions: The XPS depth profile for the SEI layers formed in each type of electrolyte was recorded for two symmetric cells after 10 cycles at 0.5 mA cm^{-2} and 1 mAh cm^{-2}. Then, sputter etching was performed using a Ar^{+} gun (2 keV 10 mA) to obtain the desired depth profile. The sputtering area was 1.3 × 1.3 mm^2, and the etching rate was 1.11 nm s^{-1} based on Ta_2O_5.

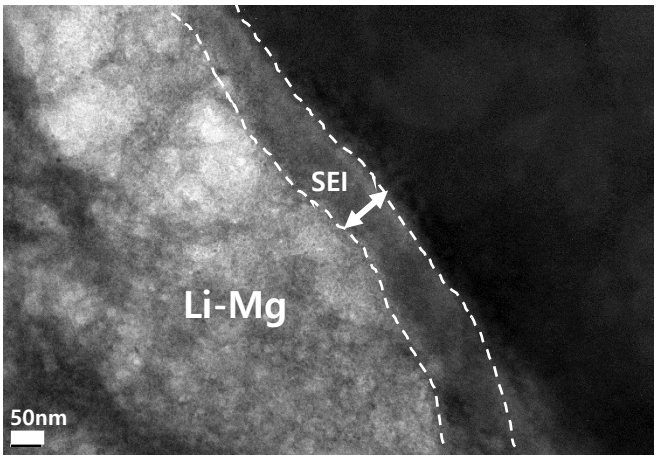

Fig. S5. TEM image of the Li–Mg alloy anode.

TEM analysis was conducted on the surface of cycled Li-Mg alloys to measure the SEI thickness. TEM analyses revealed the SEI layer formed on the surface of the Li–Mg alloy and confirmed its thickness as approximately 78 nm. The cycled Li-Mg sample was prepared using a focused ion beam (FIB) microscope (ZEISS, Crossbeam 550, Germany) for TEM observation. Pt was deposited on the sample to protect the sample surface. The sample thickness was reduced to less than 100 nm using a Ga+ ion beam for observing the SEI layer on the surface. The SEI layer formed on the surface during cycling was observed by TEM (JEOL Ltd., Tokyo, Japan, JEM-3010) with an acceleration voltage of 300 keV. The prepared TEM sample was loaded onto the TEM holder in a glove box to minimize degradation due to air exposure.

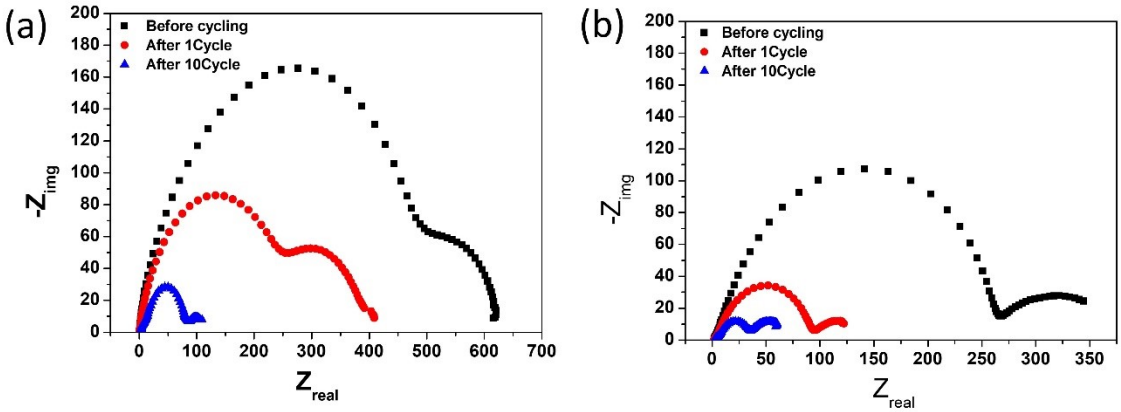

Fig S6. EIS profiles of (a) Li ‖ Li and (b) Li–Mg alloy ‖ Li–Mg alloy (*d* = 132 µm) symmetric cells.

To compare the changes in SEI impedance and charge impedances before and after cycling, Li and Li–Mg symmetric cells were fabricated, and EIS measurements were conducted. EIS measurements were performed using a ZIVE SP5 test system across a frequency range of 0.1 mHz to 1000 kHz with an AC voltage condition of 10 mV. Two semicircles were observed during the EIS measurements of the Li-ion battery. The first semicircle represents the SEI impedance, whereas the second semicircle represents the charge transfer impedance. A comparison of the EIS measurement results of the Li and Li–Mg symmetric cells indicated that both the SEI and charge transfer impedance were reduced in the Li–Mg alloy when compared to that of Li.

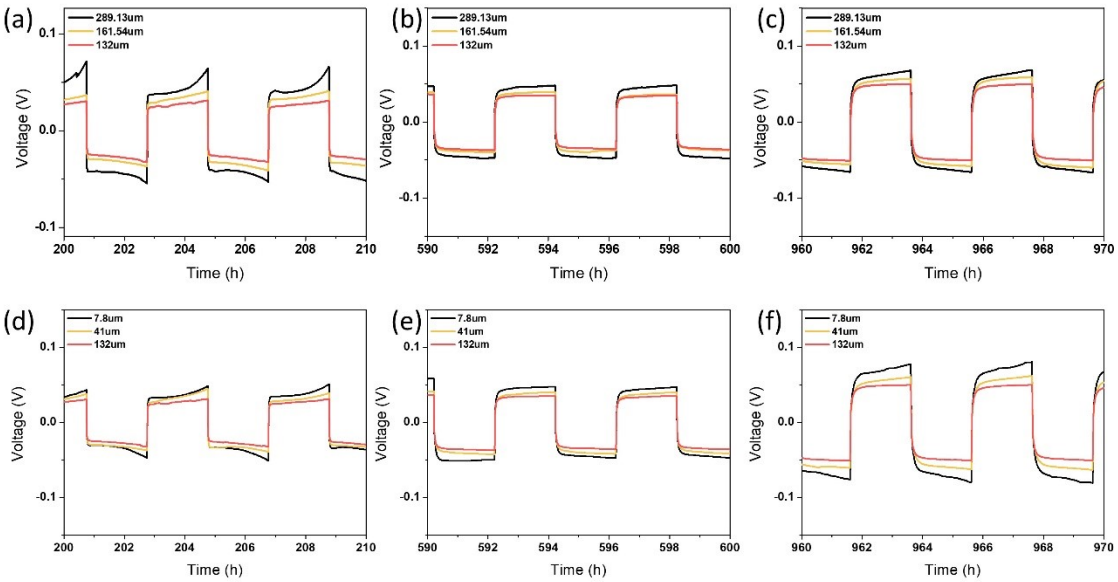

Fig. S7. Symmetric cell voltage profile.

The following results were from the cycling of the symmetric cells composed of the Li–Mg alloy at 0.5 mA cm^{-2} and 1 mAh cm^{-2}, and these results varied according to the GB density. When analyzing the voltage profile at each cycle, we observed that when the grain size was larger than 132 µm, the overpotential tended to increase. Conversely, a decrease in grain size below 132 µm also resulted in an increase in the overpotential. These findings confirm that a grain size of 132 µm in the Li–Mg alloy represents the optimal grain size.

.

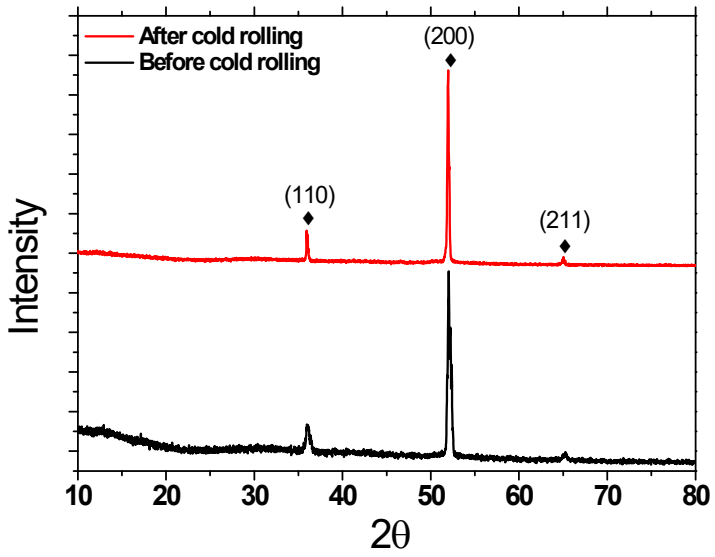

Fig. S8. Crystallographic orientation changes before and after cold rolling of the Li–Mg alloy.

The I_{110} / I_{200} ratios of the Li–Mg alloy before and after cold rolling were 0.2123 and 0.572, respectively, and the I_{110} / I_{211} ratios were 0.8755 and 1.123, respectively. These results indicated an increase in the intensity of the (110) plane following cold rolling.

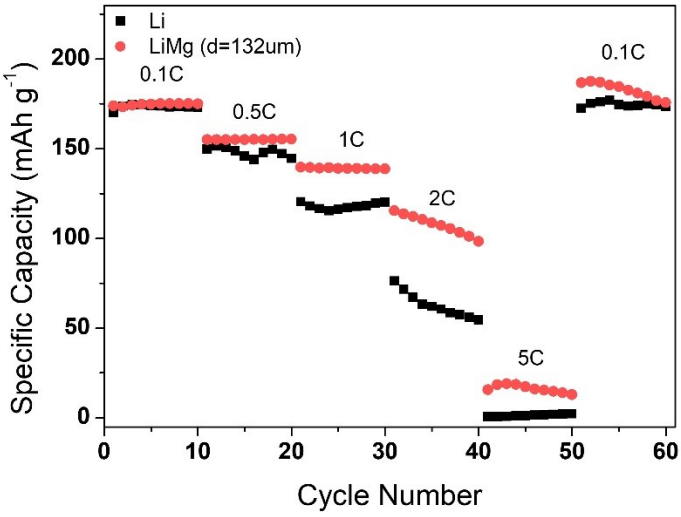

Fig. S9. Rate performance of the Li metal and Li–Mg alloy (d = 132 μm) full cells

To compare the high-rate performance of Li metal and the Li–Mg alloy with the optimized grain size, full cells were fabricated and subjected to performance testing at various C-rates. The Li–Mg alloy exhibited superior high-rate performance as compared to that of Li metal, along with superior electrochemical stability and remarkable capacity recovery. These results suggest that the Li–Mg alloy is a suitable material for next-generation energy-storage devices that involve high-rate requirements.

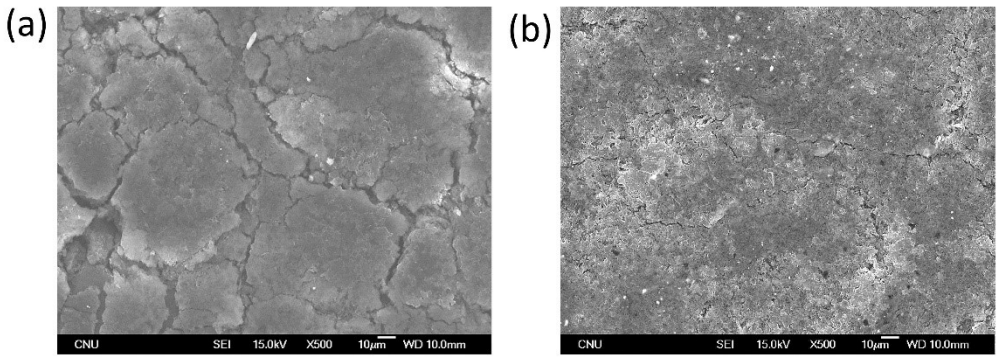

Fig. S10. SEM images of (a) Li and (b) Li–Mg alloy (d=132 μm) after cycling.

When analyzing the SEM images obtained after 500 cycles of charge-discharge testing under the condition of 0.5C, a stark difference was observed in the surface structural changes that occurred on the Li metal and Li–Mg alloy anodes. In the case of the Li metal, cycling led to the formation of cracks on its surface, severely degrading its structural integrity. In contrast, the Li–Mg alloy with a grain size of 132 μm maintained superior structural stability throughout the cycling process. These results suggest that the Li–Mg alloy maintains its structure better than the Li metal during cycling, thereby indicating a significant advantage in terms of the overall cell performance and stability.

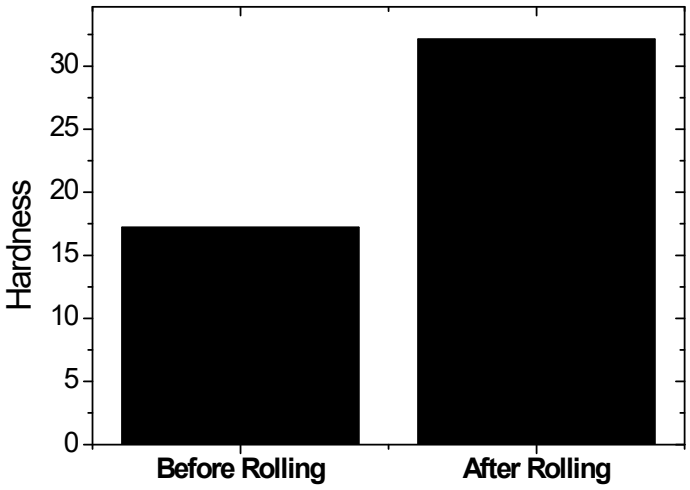

Fig. S11. Changes in Vickers hardness before and after cold rolling.

Before and after cold rolling (test load: 10 gf), the Vickers hardness values (measured using the HM-210 Vickers hardness tester (Mitutoyo, Japan)) were 17.23 HV (variation: 2.619) and 32.14 HV (variation: 2.554), respectively. This result indicated that the work hardening effect was not significant.